Michalowski, R. L. *et al.* (2018). *Géotechnique* **68**, No. 2, 133–145 [https://doi.org/10.1680/jgeot.16.P.321]

Maturing of contacts and ageing of silica sand

R. L. MICHALOWSKI*, Z. WANG† and S. S. NADUKURU‡

A typical surface texture of silica sand grains is rich in asperities and mineral debris. Consequently, a nominal inter-granular contact is composed of many 'contact points'. Associated with the contact loading process is micro-fracturing of the textural features, causing the contact to evolve. Even under a constant load, the process of micro-fracturing continues, although with a decreasing frequency. This static fatigue at contacts (or contact maturing) under a constant load is considered to be a major contributor to ageing of silica sand. The rich surface micro-morphology of silica sand grains is demonstrated using scanning electron microscopy and atomic force microscopy. Grain-scale tests indicate time-dependent deflection under constant load, attributed to delayed fracturing of textural features at grain contacts. The process is greatly dependent on the initial roughness of the surfaces. The rate of the deflection for a grain with large initial roughness (root mean square of grain surface elevation (RMS) = 621 nm), loaded with 2·4 N, was found to be 17·6 nm/h at the end of the first day after loading, whereas for a grain with approximately half the initial roughness (RMS = 321 nm) it was only about 2 nm/h. A consequence of the contact maturing process in grain assemblies is a time-dependent increase in macroscopic stiffness, and a resulting alteration of the stress state in a confined sand. This was confirmed in soft-ring oedometer tests on specimens subjected to constant load. The temporal scale of the radial stress increase in the oedometric samples was about the same as that in convergence tests on single grains. Contact maturing is accelerated by the presence of moisture and pressure dissolution, and this was manifested in tests on samples saturated with pore fluid. The results of both grain-scale and sand specimen tests are consistent with the hypothesis indicating contact maturing as the major contributor to time-dependent effects in silica sand.

KEYWORDS: particle-scale behaviour; sands; time dependence

INTRODUCTION

The response of sand to loads is typically described as an elastic–plastic behaviour with some evolution of the yield surface, which allows the hardening and softening behaviour to be captured. Such models are calibrated using macro-scale experiments (e.g. triaxial testing), and they are indispensable in engineering practice. Although useful in making engineering predictions, this phenomenological description does not reveal the nature or the cause of the behaviour. Of interest in this paper is the origin of the time-dependent behaviour of granular soils, in particular, silica sand. Time effects in sand are well documented in the literature (e.g. Afifi & Woods, 1971; Daramola, 1980; Mitchell & Solymar, 1984; Mesri *et al.*, 1990; Schmertmann, 1991; Bowman & Soga, 2003; Lade & Karimpour, 2010; Michalowski & Nadukuru, 2012; Wang & Michalowski, 2015; Wang *et al.*, 2016). This paper focuses on collecting experimental evidence in support of the hypothesis identifying static fatigue at contacts as the key cause of these effects. The term static fatigue was introduced into materials science in relation to the delayed fracture of glass (Charles, 1958). The same term was used by Scholz (1972) to describe time-dependent micro-fracturing of quartz. Because this process is affected by environmental factors, it is also referred to as stress corrosion cracking (a term often used in concrete technology). The term subcritical fracturing is used in rock mechanics to describe a similar phenomenon at the macroscopic scale.

A fair amount of research has been published on the time-dependent behaviour of soils, both sands and clays, in terms of a macroscopic response that forms the basis for phenomenological (continuum) models (e.g. Tatsuoka *et al.*, 2008; Lade & Karimpour, 2010), but much less attention has been paid to the search for mechanisms causing the time effects. Phenomena, such as growth of inter-granular bonds (Mitchell & Solymar, 1984), structuration (Mesri *et al.*, 1990; Schmertmann, 1991), force chain buckling (Bowman & Soga, 2003) or grain crushing (Lade & Karimpour, 2010; Brzesowsky *et al.*, 2014) have been cited among possible causes of ageing and rate effects, but experimental evidence has been collected mainly at the macroscopic scale (triaxial testing). Much less attention has been paid to the time-dependent processes at the scale of inter-granular contacts. Most grain-scale testing has been focused on the immediate response of grains to applied loads (e.g. Cole & Peters, 2008; Cavarretta *et al.*, 2010, 2011; Senetakis & Coop, 2013). Grain crushing at substantial loads has received a lot more attention in the literature compared to static fatigue at contacts (e.g. McDowell & Bolton, 1998; Einav, 2007; Zhao *et al.*, 2015), and this paper focuses on the time-dependent response of grains and contacts to sustained loads.

In geotechnical engineering practice, significant time dependency in sand response to loads was identified in at least two cases: gradual increase in cone penetration resistance of sand after vibratory (or blasting) compaction (Mitchell & Solymar, 1984) and time-dependent increase in shaft resistance of displacement piles or pile set-up

Manuscript received 8 December 2016; revised manuscript accepted 18 May 2017. Published online ahead of print 16 June 2017.
Discussion on this paper closes on 1 July 2018, for further details see p. ii.
* Department of Civil and Environmental Engineering, University of Michigan, Ann Arbor, MI, USA (Orcid:0000-0002-9557-4802).
† Formerly Department of Civil and Environmental Engineering, University of Michigan, Ann Arbor, MI, USA.
‡ Formerly University of Michigan, Ann Arbor, MI, USA; now Geosyntec Consultants, Keenesaw, GA, USA.

(e.g. Chow *et al.*, 1997). The former was linked to a time-dependent increase in sand strength after compaction. The authors consider the strength of sand being directly related to its fabric (and density), and conclude that the strength of sand increases immediately after the new (compacted) fabric is formed. However, the stiffness of sand will increase in time, and it will affect the stress state, producing an appearance of increasing strength in pressure-dependent soils. The increase in cone penetration resistance and pile set-up are only two, well-documented observations, but the time-dependent behaviour of sand is likely to be manifested whenever sand is freshly deposited or disturbed (and new contacts are formed).

It is believed that a major source of the time effects in silica sand at engineering stress levels is the response of inter-granular contacts to loads. This response includes time-dependent subcritical fracturing of textural features on the grain surfaces at contacts (asperities, crystalline fragments, mineral debris). The presence of moisture can accelerate this process, and an important factor in silica sand ageing is the pressure dissolution of minerals at contacts (Van Noort *et al.*, 2011) as well as chemical processes (Hu & Hueckel, 2007; Guo & Hueckel, 2015). Although air-dry contacts will be considered in grain-scale testing, the presence of moisture will be considered in testing of sand specimens.

CONTACT MATURING: A KEY CAUSE OF AGEING

Rate effects and ageing are time-dependent processes, which are ubiquitous in geomaterials. If the outcome of a test depends on time (e.g. it depends on the speed of load application), but is independent of the specific instant when the test is performed, the material behaviour is rate-dependent. For instance, visco-elastic materials are rate-dependent. If the outcome depends on the time instant when the test is performed, the material exhibits ageing. For example, concrete curing is an ageing process. Ageing of silica sand is defined here as the time-dependent process under sustained loads, leading to a change in some properties, for instance, small-strain stiffness.

The surface micro-morphology (texture) of silica sand grains is illustrated in Fig. 1. When two grains with a surface morphology as in Fig. 1 come into contact and become loaded, the predominant response is fracturing and crushing of the micro-morphological features in the contact region, causing comminution (fragmentation) of the material.

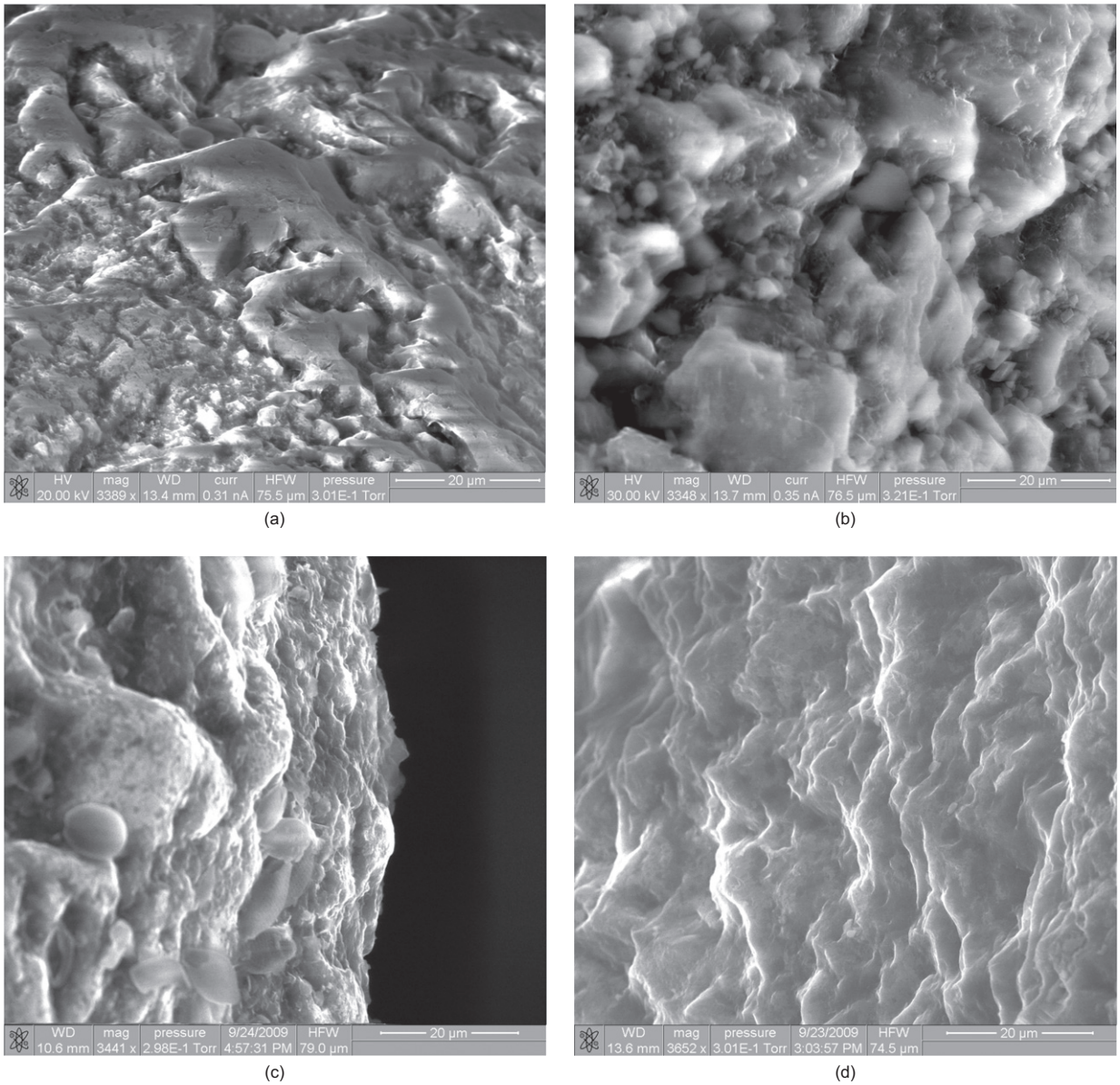

Fig. 1. Scanning electron microscopy images of surface texture of silica sand (width of images 70 µm): (a) Lake Michigan Empire Beach sand; (b) Lake Michigan dune sand; (c) Huron River (Michigan) sand; (d) Ottawa 20–30 sand

It has been argued earlier (Michalowski & Nadukuru, 2012; Wang & Michalowski, 2015) that the fracturing of the textural features on the grain surfaces at the contact does not stop after the loading process is completed; rather, it continues under sustained (constant) load, and the process is referred to as static fatigue. This process has beneficial effects on sand properties, and the term contact maturing is introduced to describe static fatigue at contacts. This is to disassociate contact maturing from the negative connotation of fatigue.

Contacts evolve during the maturing process. The authors hypothesise that this process leads to an increase in the number of contact points within a nominal contact area. Consequently, the contact becomes firmer and its stiffness increases. The authors consider contact maturing as a key cause contributing to time effects in sand. This paper is focused on collecting experimental evidence in support of the contact maturing hypothesis. This hypothesis finds its physics underpinning in the rate process theory and fracture kinetics (e.g. Glasstone *et al.*, 1941; Krausz & Krausz, 1988; Bažant & Pang, 2007).

GRAIN-SCALE TESTING

Fracture kinetics indicates that fracturing occurs as a time-dependent process under constant load, but the probability of fracture initiation and crack propagation will diminish with time. In this section, experimental evidence is sought for time-delayed response of a single contact. Two experiments are presented: (*a*) qualitative demonstration of the time-dependent relative displacement of two grains; (*b*) quantitative measurements of time-dependent convergence of two platens loading a single grain. Both experiments are conducted under constant load (constant contact force).

Contact between two sand grains

The inter-granular contacts in sand are not Hertzian contacts with well-defined geometry and elastic properties; rather, they comprise many contact sub-areas (or 'contact points') with a rich surface texture at various spatial scales, Fig. 2. Asperities on surfaces of grains in contact take an active role in the load transfer, but mineral debris present at contacts can also participate in grain-to-grain load transfer, Fig. 2(d). During the loading process some of these microscopic features will be fractured or crushed, leading to a firmer contact. Hypothetically, this firming is associated with an increased number of 'contact points', and will be manifested as larger contact stiffness. Examples of contact regions on grains are illustrated in Fig. 3. The first pair of images demonstrates a contact region before loading and after it was

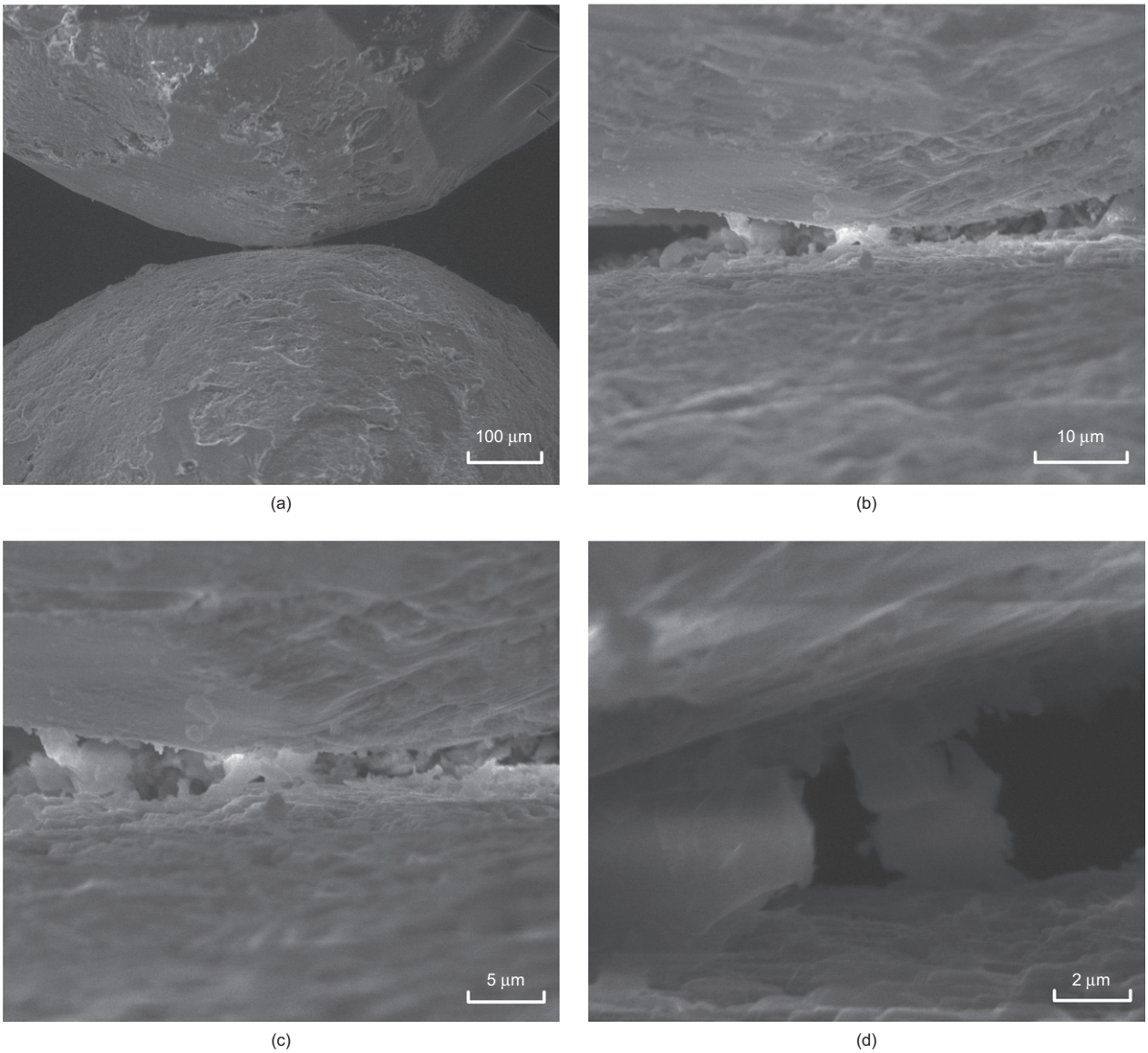

Fig. 2. Air-dry contact between two silica sand grains at different spatial scales

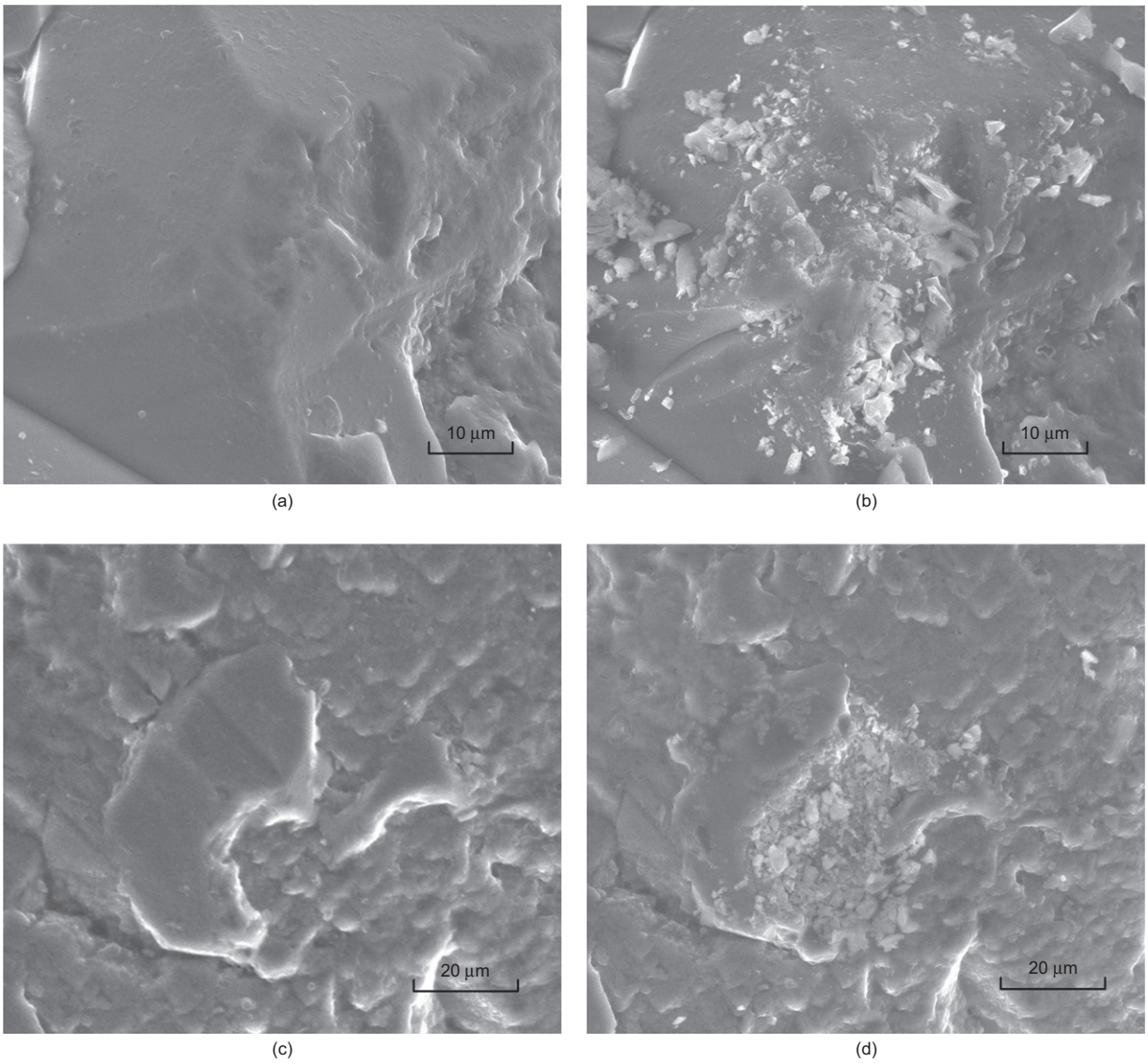

Fig. 3. Examples of two contact regions before and after loading: (a) inter-granular contact region before loading; (b) after loading with a force of 3 N for 3 days; (c) kidney-shaped feature at a contact between a grain and a glass plate; (d) after loading with a force of 0·7 N for 7 days

loaded with a force of 3 N for 3 days. There is a noticeable fracture close to the lower-left corner in Fig. 3(b), and the region is covered with debris produced during fracturing. The second pair of images shows a kidney-shaped feature before and after loading with 0·7 N for 7 days. The process led to crushing and comminution of a section of the kidney-shaped feature. While contacts evolve during loading, the process of micro-cracking and crack propagation continues even after the load no longer increases. The following is a demonstration that an inter-granular contact loaded with an oblique force does not remain stationary, even under a constant load; rather, the grains will displace with respect to one another in time, with a decreasing rate.

Demonstration of time-dependent response of two grains in contact

A small vice was used to load a contact between two grains, Fig. 4, and the relative displacement of the grains was observed using a scanning electron microscope (SEM). The grains were bonded to specially shaped SEM pin stubs using a conductive silver adhesive, and the required force was induced by a calibrated spring pressing against a movable reaction plate, as illustrated in Fig. 4. The vice had

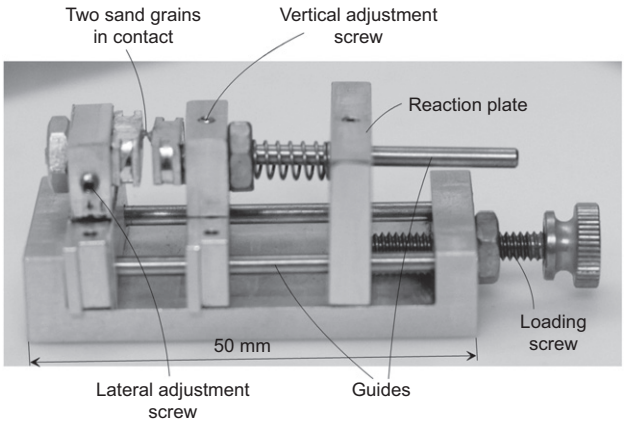

Fig. 4. A vice for loading two grains in contact

micro-screws, allowing alignment of the two grains, so that the contact could be loaded with either an approximately normal or an oblique force.

Two Ottawa sand grains (grain size between 0·6–0·84 mm) were loaded with a force of 2·5 N, and the entire assembly

was periodically placed in the SEM chamber to record the image of the relative position of the two grains. The force was applied at an oblique angle to the contact, with the shear component expected to cause relative sliding in addition to normal convergence of grains. The exact obliquity could not be determined for two reasons: (*a*) true contacts between grains do not have one well-defined normal, and (*b*) the contact area was not in direct SEM view (it was obscured by the body of the grain). The four images in Fig. 5 show the relative configuration of the grains 10 min after the load was applied, and then after 2, 3 and 9 days. The black dashed line indicates the contour of the upper grain. One point is marked on the stationary (lower) grain (circular bullet) and two points on the moving grain to visualise the extent of the relative motion. The quality of these images was compromised by the geometry of the loading set-up, which made it difficult to capture the electron beam reflected from the grain surfaces; still, the images clearly indicate that the configuration of the two grains subjected to a constant load did not remain stationary. The upper grain is gradually changing its position in the down–right direction over the stationary bottom grain. The projection of the distance travelled by the point marked with a black base triangle was about 300 μm in 9 days after application of 2·5 N. The rate of relative displacement was initially large, but this rate decreased with time (decaying process); that is, the displacement between days 3 and 9 is a lot smaller than that between days 2 and 3. A normally loaded contact would be expected to retain its location on the grain surfaces, and the grains would undergo only normal convergence. However, the contact was loaded with an oblique force and so it shifted in the process. This qualitative test was performed solely as a demonstration of time-dependent kinematics of two grains in contact, subjected to a constant load.

Quantitative measurements of contact response

A time-dependent response of a contact between two grains was reported in Michalowski & Nadukuru (2014). However, such results are always burdened by inaccuracies. This is because the grains need to be mounted on opposing loading platens, and no matter how they are mounted, the measured response is always a combined response due to static fatigue process at the contact between the grains and the two contacts between the grains and the loading platens (including the mounting glue). This is why it was decided to test one grain, load it through two steel platens, and measure the combined (simultaneous) response of two contacts of this grain with relatively rigid and smooth surfaces. Part of the time-dependent response to sustained load comes, of course, from the creep of the core material of the grain. This cannot be avoided, but an estimate of this component of the response will be made using a test on a relatively smooth borosilicate glass bead. Even though the response of two contacts of a

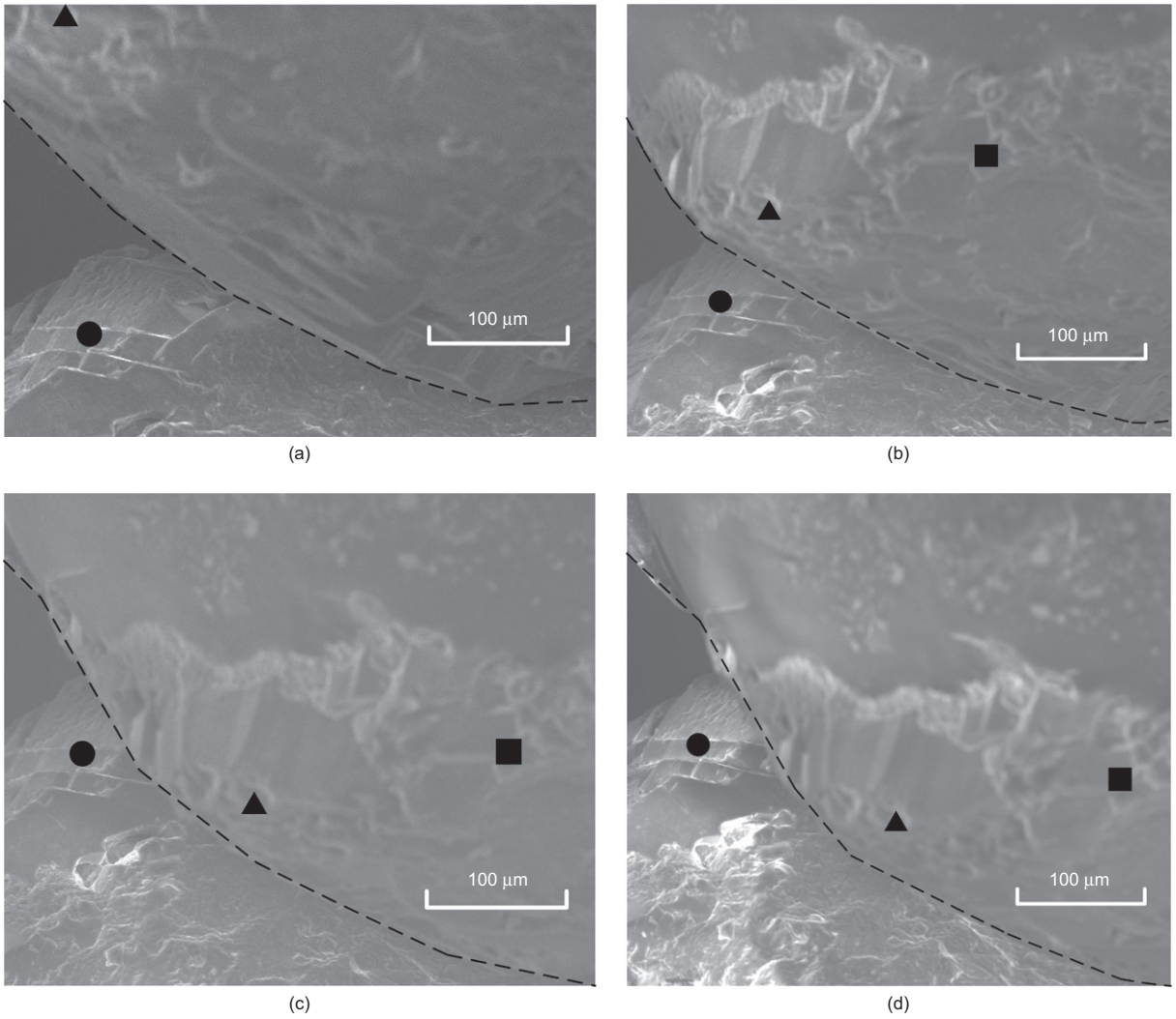

Fig. 5. Qualitative test – relative displacement of two grains in contact subjected to an oblique constant force of 2·5 N: (a) 10 min after load application; (b) after 2 days; (c) after 3 days; (d) after 9 days

grain with two surfaces of low roughness is not equivalent to a contact between two grains, it is still very much indicative of the contact behaviour. The advantage of simultaneous testing of two contacts on one grain is in eliminating the uncertainties in measurements, which are associated with the response of glue and the mounting contacts present in two-grain tests, and also eliminating uncertainties related to the obliquity of the contact normal.

To obtain quantitative data the device in Fig. 6 was constructed. The apparatus has a stage (mounted on a square bracket) with one degree of freedom in the vertical direction. Three potentiometers (Novotechnik TR 10A102) are mounted on the stage. A grain is placed between a polished steel SEM stub and the polished surface of a steel head of the potentiometer arm (both referred to as platens). The central potentiometer has a calibrated spring, and is used to apply the required force (spring constant $k = 0{\cdot}447$ N/mm). Once the required force is reached by adjusting the micrometer on the stage, this potentiometer reads the time-dependent change in relative distance between the platens loading the grain, referred to here as convergence. The record is collected with the frequency of 1 Hz, using a data acquisition system with components manufactured by National Instruments. The system was housed on a compact chassis (NI cDAQ-9178). Potentiometers were powered by a four-channel 16-bit analogue voltage output module (NI 9263). Two four-channel 24-bit analogue modules (NI 9219) were used to measure the output voltage from the potentiometers, as well as the supply voltage (nominally 0·5 V). Even though the stage is designed to move in the vertical direction only, the tolerances in the stage rails allow for minute rotations, and the remaining two potentiometers are used to detect any rotation that might occur (ideally, the two symmetrically placed potentiometers read zero displacement during the constant-load test). The convergence measured is attributed to the static fatigue process at the two contacts of the grain with the two loading platens, with some portion coming from the creep of the core material of the grain. This will be confirmed later with a test on a relatively smooth borosilicate glass bead. Because of the sensitivity of the micro-fracturing process to environmental factors, the apparatus was placed in an environmental chamber where constant temperature (20 ± 1°C) and relative humidity (30 ± 5%) were maintained.

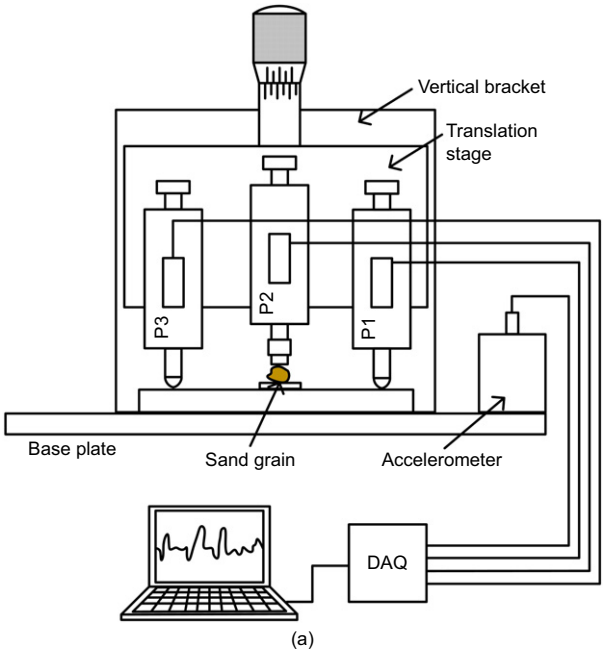

(a)

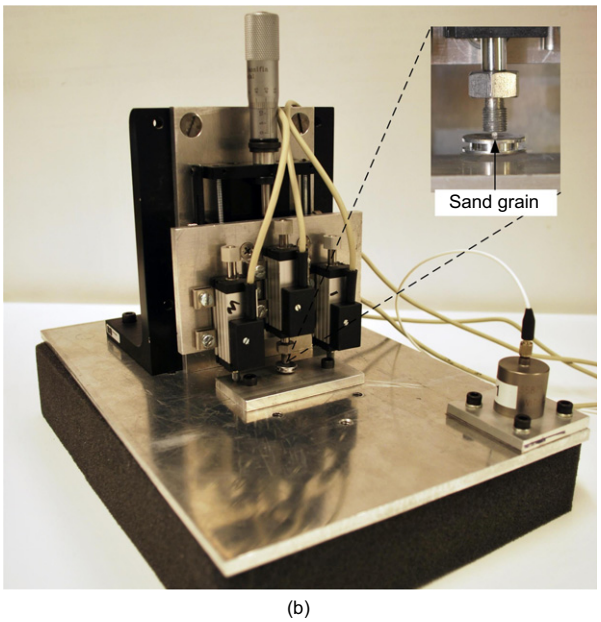

(b)

Fig. 6. Grain-scale testing apparatus: (a) schematic diagram; (b) view of the device

The richness of the surface texture can be quantified using atomic force microscopy (AFM), and can be described with the root mean square (RMS) of the surface elevation measured by AFM, defined as

$$\mathrm{RMS} = \sqrt{\frac{1}{mn}\sum_{i=1}^{m}\sum_{j=1}^{n}\left(z_{ij}-\mu\right)^2} \tag{1}$$

with μ being the average elevation of the surface, calculated as

$$\mu = \frac{1}{mn}\sum_{i=1}^{m}\sum_{j=1}^{n} z_{ij} \tag{2}$$

where m and n are the number of points in the scan in the x and y directions, respectively, and z_{ij} is an elevation located by the ith and jth point in the x and y direction, respectively. It is emphasised that this method was used to describe the initial roughness, but not to characterise the evolution of roughness as a result of contact maturing. The latter was not attempted because of technical difficulties with restarting the test with the same grain after taking AFM measurements. Therefore, the RMS calculated needs to be interpreted as the initial root mean square of the grain surface elevation. Another issue in characterising the roughness of the grain surface at contacts is associated with variability of roughness on a single grain. Grains selected for testing were first inspected using SEM, and those with a relatively uniform roughness were chosen. AFM scans included a 30 μm square that was believed to be representative, but the actual contacts were formed at the time of load application. Consequently, the RMS calculated based on the AFM scans needs to be understood as an approximate measure of the initial roughness, and not as the exact roughness at the contact. A Veeco Dimension Icon atomic force microscope was used for all scans.

First, a test was performed on a high-molybdenum stainless steel sphere, 3·175 mm in diameter (surface initial roughness measured by RMS = 39·5 nm), loaded with a force of 1·3 N, for nearly 6 days, Fig. 7. The signal indicates a small 'adjustment' of the sphere to the applied load in the first day (about 70 nm), and no time-dependent convergence

thereafter. A distinct convergence was not expected in this case, because of the absence of significant roughness and high material strength (negligible static fatigue at the contacts). The inner band in Fig. 7 shows the signal filtered with a Savitzky & Golay (1964) filter.

Grains for testing were selected from a batch of Ottawa sand grains, with a size in the range of 0·6–0·84 mm (Ottawa 20–30). The degree of roundness of these grains was described as 'rounded', with a numerical value of roundness estimated as from 0·65 to 0·7 according to the Krumbein (1941) chart. Grains with a relatively uniform roughness (inspected by SEM) were selected for testing. Initial roughness of individual grains was characterised by the RMS (equation (1)) as calculated from AFM scans. Figure 8 shows AFM scans of one loading platen and four grains used in the tests. This figure also indicates the RMS value for each scan, and it shows a representative cross-section of the scans to further visualise the initial surface texture.

Testing was performed at a constant temperature of 20 ± 1°C and low relative humidity of 30 ± 5%, to avoid the influence of a change in silica volume due to moisture penetration (Wiederhorn *et al.*, 2014). Results from tests on four grains (including two tests on one grain, but different load and contacts) and one spherical borosilicate glass bead are shown in Fig. 9. In each test, the loading to the required contact force occurred in four equal steps, with a 2 min pause between the steps. The convergence in Fig. 9 is set to zero at 30 min after the loading started. The time-dependent convergence appears to be primarily reliant on the initial roughness of the grain surfaces (as measured by RMS) and on the load. The signal band from the potentiometer was reduced with a moving average filter with a five-point span, which reduced the noise band from over 100 nm down to about 50 nm.

The sand grains were loaded with a force of either 2·4 N or 1·3 N. The convergence after the load application ranged between 18 and 67 μm (Table 1), dependent on the roughness and the load. Test C displayed an immediate convergence that was larger than expected, considering the trend in all tests presented. The loading process of this grain exhibited unusually large convergence after the first loading step (27 μm), which was likely caused by an 'adjustment' of the grain to applied load (minute grain rotation). The time-dependent convergence for all grains that occurred in the 20 days following application of the load was one to two orders of magnitude smaller than the immediate response.

The summary of the tests is given in Table 1. Grains in tests B, C and E were all loaded with a force of 2·4 N, but had different initial roughness measured by the RMS: 28·6 nm, 321 nm and 621 nm, respectively. Not surprisingly, the largest convergence was recorded for test E, with the largest roughness, and the smallest for test B. The convergence after 20 days for tests B, C and E was 310 nm, 780 nm and 2385 nm, respectively. A similar conclusion regarding the strong influence of initial roughness on convergence comes from the two tests with 1·3 N load: A and D, with roughness of 28·6 nm and 577 nm, respectively. Convergence after 20 days for the two tests was recorded as 100 nm and 1090 nm, respectively. The strong role of the roughness in the convergence process is confirmed by comparison of tests D and B: even though test D was performed under 1·3 N load (2·4 N in test B) it showed a larger convergence, because of a much larger initial roughness (577 nm as opposed to 28·6 nm).

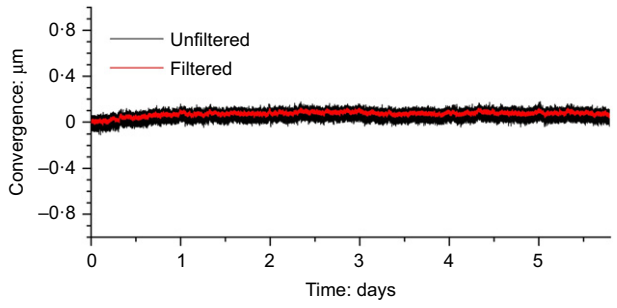

Fig. 7. Time-dependent relative displacement (convergence) of two platens loading a stainless steel sphere (3·125 mm in diameter) with a force of 1·3 N

The convergence is a decaying process, still strongly dependent on initial roughness in the first few days. Calculated based on data in Fig. 9, the convergence rate was about 17·6 nm/h at the end of the first day for the grain with initial RMS = 621 nm (test E), but only a little above 2 nm/h for roughness of 321 nm (test C) and below 2 nm/h for roughness of 28·6 nm (test B). It is interesting to note that the first-day rate in test D was relatively high despite a lower load (1·3 N): 6·9 nm/h; this is presumably due to a relatively large initial roughness of 577 nm. After 20 days, the convergence rate for all tests dropped below 1 nm/h; this rate is likely to have a significant component due to creep of the core material in the grain.

An approximately constant and low rate of convergence reached in tests A and B shortly after loading is likely indicative of the process being strongly influenced by the creep of the core material of the grain, rather than static fatigue at the contacts. To obtain some quantitative measure of the influence of creep, an 8 day test was performed on a silicate sphere (diameter 2·38 mm) with very low roughness (RMS = 6·28 nm). The sphere was made of borosilicate glass, with about 80% silicon dioxide (SiO_2) (manufacturer's specification: 70–87% silicon dioxide). The time–deflection response of the glass bead is shown in Fig. 9(b) (test F). Loaded with 2·4 N, the convergence exhibits some 'adjustment' in the first day, possibly due to fracturing of some asperities despite the low roughness, but the rate of convergence drops to about 0·1 nm/h after 2 days. This low-rate process is likely to be the effect of creep of the bead core material (a smaller bead would likely exhibit lower rate of convergence). The measurements for tests A, B and F in Fig. 9(b) are within the raw noise of the signal, but the filtered results are repeatable. Comparison of the bead data and the data for the tests with low roughness (tests A and B) leads to the conclusion that the convergence in tests A and B is indeed influenced by the creep of the grain core material. This is consistent with the initial roughness profile of the grain in tests A and B (Fig. 8(b)) compared to those in tests C, D and E (Figs 8(c)–8(e)); that is, one would not expect substantial static fatigue occurring at contacts for the grain in tests A and B. Of course, creep of the grain material affects the convergence process from the very beginning, but it presents a very small component of convergence for grains with large roughness where static fatigue is the predominant process in the first several days after loading.

Occasionally a spike or a 'jump' in the signal was recorded. These can come from disturbances in the power supply, the stick–slip movement of the slider inside the potentiometer, or they can be caused by external excitation. However, they can also be triggered by contact micro-instabilities associated with sudden fracture of asperities and mineral fragments, or a minute rotation of a grain between the platens. An accelerometer was mounted on the base plate in order to detect external disturbances (probing at 2 kHz). The spike in the reading of test D just past 20 days, Fig. 9(a), was likely to have been caused by an electrical issue, but the jump in the test C curve just past 7·1 days was likely caused by external excitation, which was documented in the accelerometer record. The size of an acceleration record from a single test

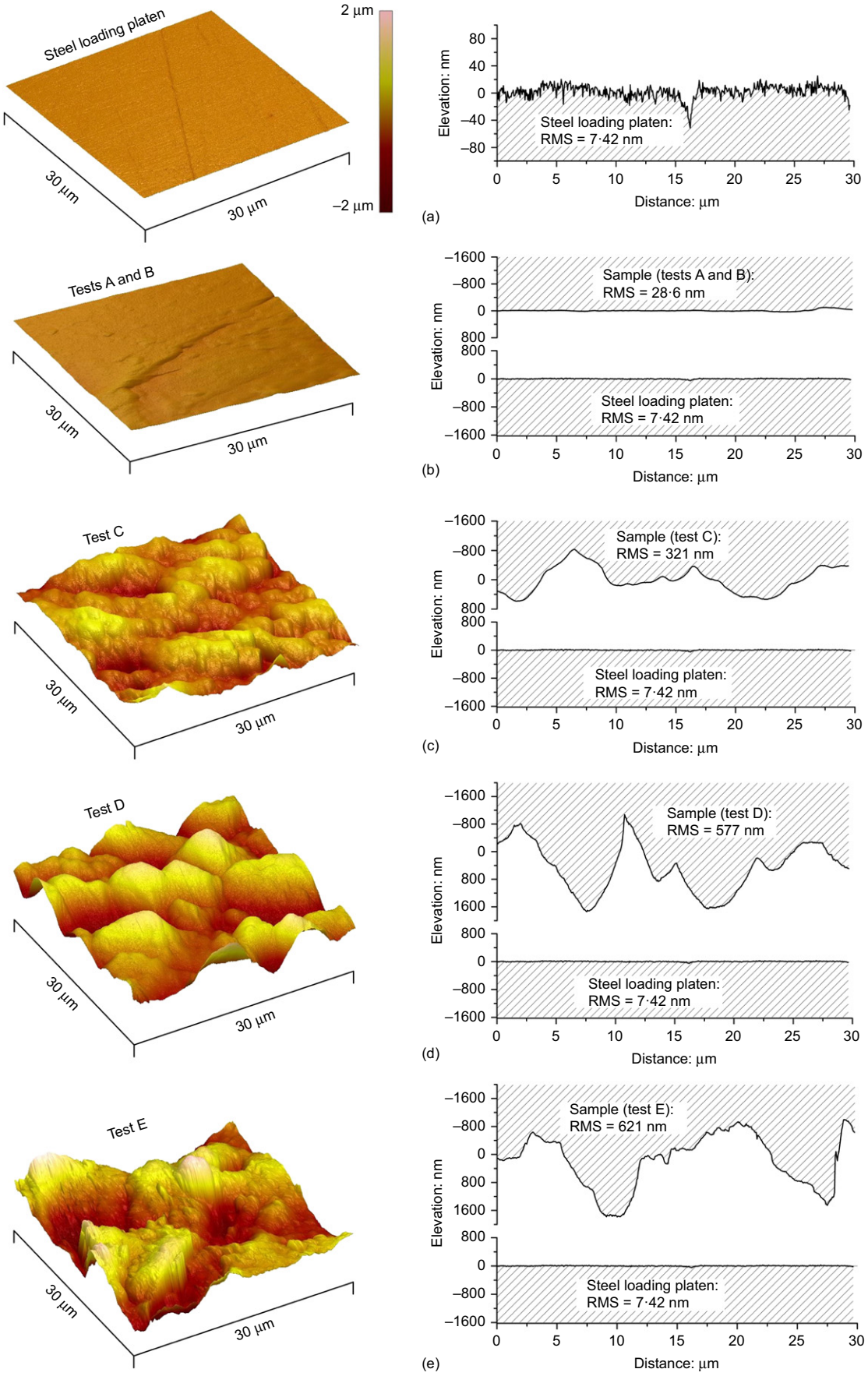

Fig. 8. Atomic force microscopy scans of grains used in testing: (a) steel surface of a loading platen, RMS = 7·42 nm; (b) sand grain with RMS = 28·6 nm; (c) RMS = 321 nm; (d) RMS = 577 nm; (e) RMS = 621 nm

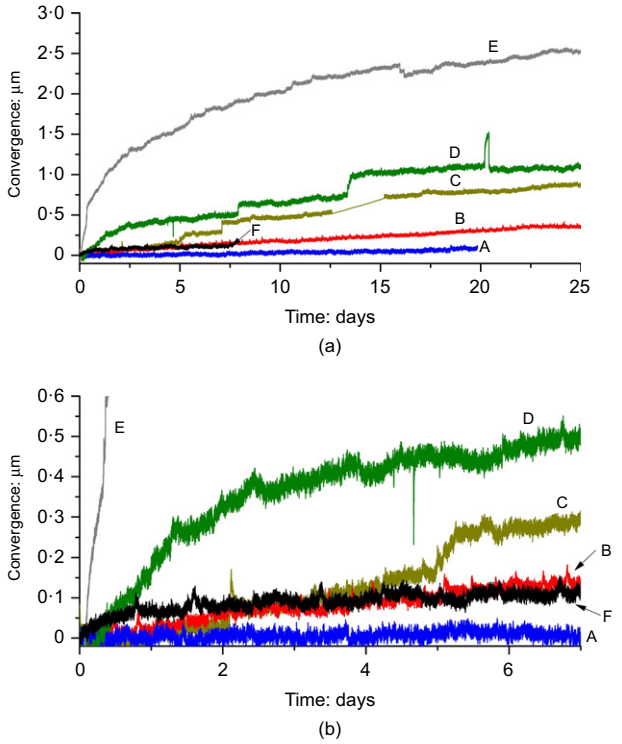

Fig. 9. Grain-scale tests: (a) time–deflection response of single grains (convergence); (b) enlarged 7 day section with borosilicate glass bead deflection (A, load 1·3 N, RMS = 28·6 nm; B, load 2·4 N, RMS = 28·6 nm; C, load 2·4 N, RMS = 321 nm; D, load 1·3 N, RMS = 577 nm; E, load 2·4 N, RMS = 621 nm; F, load 2·4 N, RMS = 6·28 nm, borosilicate glass bead)

is of the order of tens of GB, and it is not practical to plot it to match the test duration in Fig. 9 (the records indicate the noise of $\pm 0{\cdot}02\boldsymbol{g}$).

A straight line on the test C curve between 12·5 and 15 days is due to an interrupted power supply during that time. These anomalies in long-term testing were found to be unavoidable.

CONSEQUENCES OF CONTACT MATURING IN CONFINED SAND

It is the hypothesis advocated in this paper that fracturing of textural features on grain surfaces at inter-granular contacts leads to an increase in the number of 'contact points' (or 'contact sub-areas') within a nominal contact area. This is a plausible mechanism causing an increase in the contact stiffness, which would also be manifested as an increase in the small-strain stiffness at the macroscopic scale. This increase in stiffness is a key consequence of sand ageing. In a confined mass, a change in stiffness is likely to cause a change in the stress state. This manifestation of contact maturing was investigated using soft-ring oedometer tests. It is important not only to detect the evolution of the stress state, but also to estimate the temporal scale of the process. If this temporal scale matched the scale of the contact maturing process, then it would be reasonable to expect that contact maturing might play a key role in sand ageing.

Consider a cylindrical specimen, such as the one in an oedometer test, loaded in the vertical direction with uniform load, q. Such a load will induce vertical, radial and circumferential stresses in the sample: $\bar{\sigma}_z$ (equal to q), $\bar{\sigma}_r$ and $\bar{\sigma}_\theta$, respectively; because of axial symmetry, $\bar{\sigma}_\theta = \bar{\sigma}_r$. The bar indicates that these are averaged stresses in the granular material. Barring any shear stresses at the top and bottom platens, and on the oedometer cylinder, stresses $\bar{\sigma}_z$, $\bar{\sigma}_r$ and $\bar{\sigma}_\theta$ are the principal stresses. Although the response of the granular material to loading can be characterised as both elastic and irreversible deformation, consider only a purely elastic process. The energy accumulated in an isotropic specimen while it is loaded from zero to q is

$$W_e = \frac{1}{2E}\left(\bar{\sigma}_z^2 + \bar{\sigma}_r^2 + \bar{\sigma}_\theta^2\right) - \frac{v}{E}\left(\bar{\sigma}_z\bar{\sigma}_r + \bar{\sigma}_r\bar{\sigma}_\theta + \bar{\sigma}_\theta\bar{\sigma}_z\right) \qquad (3)$$

where $\bar{\sigma}_z = q$, and E and v are Young's modulus and Poisson ratio, respectively. Assume now that, after the specimen was loaded, the stiffness of the material expressed by Young's modulus E increases (with Poisson ratio remaining constant). This is to account for the increase in the macroscopic stiffness that was caused by the increase in the stiffness of maturing contacts. Consistently with equation (3), an increase in Young's modulus would lead to a decrease in energy stored in the specimen. Because load q is kept constant, stresses $\bar{\sigma}_r$ and $\bar{\sigma}_\theta$ would have to increase in order to preserve the strain energy. Sand, of course, is not a purely elastic material, and a substantial amount of energy is dissipated during the loading process. Under constant load, some energy may be changed into heat in the frictional process of inter-particle sliding during the 'structuration' events, and a portion of energy may be emitted as elastic waves (micro-seismicity) produced by fracturing during the static fatigue process. However, if the conjecture regarding the increase in stiffness caused by contact maturing is true, then it is likely that some increase in the radial and circumferential stresses will occur in time. To confirm this supposition a soft-ring oedometer testing programme was carried out.

SOFT-RING OEDOMETER TESTING

The purpose of soft oedometer testing is collecting additional evidence for the time-dependent response of silica sand to constant loads, and demonstrating the consequences of contact maturing on the response of confined sand.

Table 1. Summary of contact maturing tests

Test	RMS: nm	Contact force: N	Test duration: days	Convergence 30 min after loading started: μm	Time-dependent convergence		
					After 1 day: nm	After 5 days: nm	After 20 days: nm
A	28·6	1·3	20	18	5	10	100
B	28·6	2·4	25	39	10	100	310
C	321	2·4	25	67	25	210	780
D	577	1·3	25	22	170	451	1090
E	621	2·4	25	60	845	1582	2385
F*	6·28	2·4	6	21	70	99	—

*Borosilicate glass bead

Friction between the specimen and the oedometer ring will influence the outcome of the stress measurements (e.g. Rohe *et al.*, 2009). Similarly, the relatively low stiffness of the ring will influence the radial stress in the specimen. However, the magnitude of the radial stresses incurred from the circumferential strain of the ring is not central to these experiments. Of primary importance is the time scale of the process, and an observation as to whether or not the intensity of radial stress increase in the oedometer and the convergence increase in the grain-scale experiments are of the same temporal scale. If they were, then it would be reasonable to expect that silica sand ageing is related to contact maturing, a hypothesis advocated in this paper.

Soft oedometer ring and experimental set-up

A 'soft oedometer' (Kolymbas & Bauer, 1993) allows measuring of radial stresses induced in a specimen by applied vertical loads. In a thin-walled elastic ring, an increase in the circumferential strain in the ring is uniquely related to an increase of the radial stress in the specimen. The aluminium rings used in the tests had a thickness of 0·1 mm, and their circumferential strain was measured by two strain gauges mounted on the exterior of the ring (located on the ring perimeter at 180° from one another). The small thickness of the ring provided elastic deformability, allowing detection of small changes in radial stress (about 100 Pa). The data acquisition system now included an additional strain/bridge input module (NI 9237) used to take voltage readings from the strain gauges (four-channel, 24-bit analogue simultaneous sampling data acquisition module). The soft ring was placed on a mirror-finish stainless steel base plate to reduce the friction between the ring and the specimen, and the base.

The diameter of the rings was 66 mm, and the height was 50·8 mm (25·4 mm in tests with stainless steel spheres). The settlement of the specimen was measured with a potentiometer at frequency 1 Hz, whereas the signals from two gauges measuring the circumferential strain of the ring were recorded at 0·05 Hz. The entire assembly was placed in an environmental chamber where a constant temperature of 20 ± 1°C and constant relative humidity of 30 ± 5% were maintained. The influence of temperature on the rate of static fatigue was not part of this study, and the temperature of 20°C was selected because opening of the chamber door during tests (which was necessary for resetting the equipment after an occasional power failure) produced a small disturbance in the temperature. An accelerometer was mounted on the base of the oedometer frame to record any accidental disturbances/vibrations (data recorded at 2 kHz).

Air-dry and saturated samples were tested. To avoid drying out of the saturated samples, a constant-head reservoir with appropriate supply of the pore liquid was used to allow a 3 week test to be run without entering the chamber to replenish the pore fluid.

Stainless steel spheres test

In order to test the robustness of the soft-ring test, an experiment was first performed on a sample comprising uniform stainless steel spheres with a diameter of 3·175 mm (high-molybdenum E52100 alloy). The specimen was assembled in the soft cylinder by discharging spheres from a funnel kept at the smallest height above the specimen that still allowed the discharge. Porosity of the prepared specimen was 0·41, the specimen was loaded to an average vertical stress of 118·3 kPa in four equal steps (in 2 min intervals), and the load was maintained for 7 days. Because the stainless steel has a high yield stress and the reflective finish has a low roughness, contact maturing was not expected to be noticeable under applied loads, as was already indicated in the single-grain test, Fig. 7. Therefore, consistent with the contact maturing hypothesis, contact stiffness and macroscopic stiffness were not expected to increase, and the radial stresses under a sustained load were expected to remain constant.

After application of 118·3 kPa in the axial (vertical) direction, the radial stress increased to slightly over 116·5 kPa, stabilised within the next hour at about 116·7 kPa, and remained constant for the duration of the test (nearly 7 days), Fig. 10(a). It is not surprising to notice that the macroscopic stress state was nearly hydrostatic in the assembly of reflective-finish stainless steel spheres. No time-dependent increase in macroscopic radial stress of the steel spheres assembly was taking place and, therefore, it was concluded that no increase in contact stiffness was taking place during the sustained load. Indeed, static fatigue was not expected to occur on reflective-finish steel surfaces, whereas contact maturing is what the authors consider as the key process in sand ageing. The stainless steel spheres specimen did not display any signs of ageing in 7 days.

Thirty minutes after the application of the load, the settlement was 281·5 μm, which yields a vertical strain of a little over 1%. The settlement increased by less than 3 μm within the first day, stabilised at about 284·3 μm and remained at this level for the next 6 days, Fig. 10(b).

Sand tested

The results are presented for three types of sand: Ottawa 20–30 sand, Lake Michigan Empire Beach sand, and Lake Michigan dune sand. The representative d_{50} grain size is 0·74 mm, 0·34 mm and 0·23 mm for the three sands, respectively. Ottawa 20–30 sand is quite uniform (poorly graded, with grain sizes between openings of mesh #30

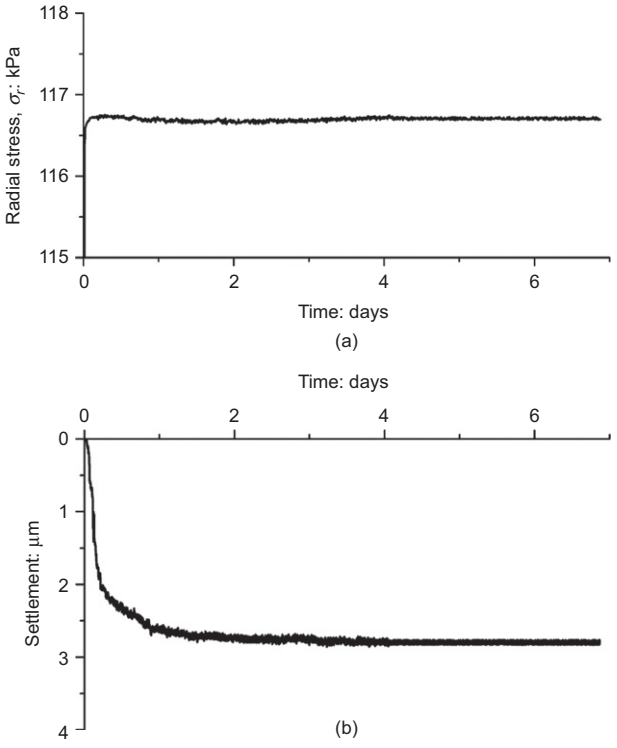

Fig. 10. Soft oedometer test with stainless steel spheres (3·125 mm in diameter); vertical load 118·3 kPa, ring height 25·4 mm: (a) radial stress as a function of time and (b) settlement

and #20, i.e. 0·6 and 0·84 mm). For Ottawa sand, the coefficient of uniformity $C_u = 1{\cdot}07$ and coefficient of curvature $C_c = 0{\cdot}99$; for Lake Michigan dune sand: $C_u = 1{\cdot}53$ and $C_c = 1{\cdot}16$; and for Lake Michigan Empire Beach sand: $C_u = 3{\cdot}39$ and $C_c = 0{\cdot}87$.

Air-dry samples were prepared by discharging the sand from a funnel with an opening diameter of 8 mm, from a height of 1 cm. All sand specimens were assembled in a 50·8 mm tall ring. Prior to Ottawa sand sample preparation, the sand was subjected to sieving, and any traces of fraction smaller than 0·6 mm (sieve #30) and larger than 0·84 mm (sieve #20) were removed. Sieving was repeated after each test, and anywhere between 0 and 1% of fraction smaller than 0·6 mm was found. This is indicative of no grain fracturing to very minor grain splitting.

Results and observations from testing

Six test results are presented in Fig. 11, three air-dry specimens of all sands, and three Ottawa sand specimens saturated with distilled water and a sodium hydroxide (NaOH) water solution (pH = 11). The duration of the tests reported varied from 12 to 20 days. It was common for the tests to be terminated because of a power surge or external excitation that made further readings unreliable. The signal in Fig. 11 is not filtered.

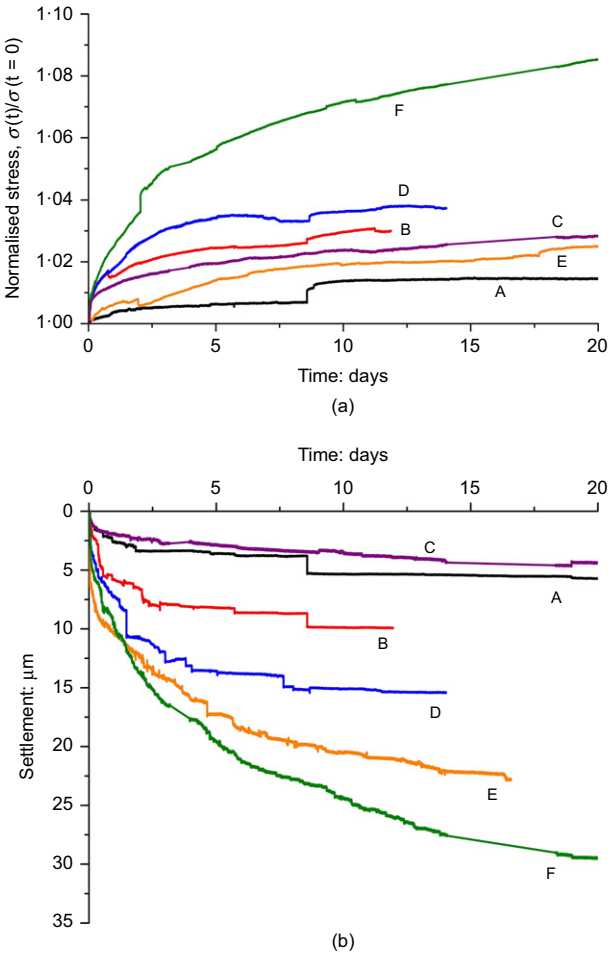

Fig. 11. Soft-ring oedometer test results: (a) normalised radial stress plotted against time; (b) settlement plotted against time (A, Ottawa sand, dry, 230 kPa; B, beach sand, dry, 230 kPa; C, dune sand, dry, 230 kPa; D, Ottawa sand, distilled water, 230 kPa; E, Ottawa sand, distilled water, 345 kPa; F, Ottawa sand, pH = 11 sodium hydroxide solution, 230 kPa)

All but one specimen were loaded to an average stress of 230 kPa, and one to 345 kPa; loading occurred in four equal steps, every 2 min, which resulted in the completion of the entire loading process in about 10 min. The immediate settlement varied from about 260 to 560 μm (from 0·5 to 1%), whereas the time-dependent settlement in the following 12 days reached about 4 to 26 μm. These results are summarised in Table 2, and the time-dependent processes of increasing radial stress and increasing settlement are shown in Figs 11(a) and 11(b), respectively. The data in Fig. 11 are plotted starting 30 min after the loading process began, and the radial stress in Fig. 11(a) is normalised by its value at 30 min, as given in the sixth column of Table 2.

The largest immediate settlement occurred for the beach sand (test B), despite a slightly lower porosity than the other samples (Table 2). However, the longer-term process is affected the most by the presence of pore fluid. Earlier research indicated dissolution of silica in water, with the largest rate of the process in alkaline solutions (Krauskopf, 1959). This dissolution process causes accelerated static fatigue of silica (Charles, 1958), which affects both the rate of the radial stress increase and the rate of settlement increase. As expected, of two Ottawa sand specimens saturated with distilled water and loaded to 230 kPa and 345 kPa (tests D and E), the one with the larger load (E) exhibited larger immediate settlement and larger long-term settlement, but not as large as the specimen with a lower load (230 kPa) and saturated with alkaline solution (F). Although the absolute value of the radial stress is the largest in the specimen loaded to 345 kPa (test E), the normalised time-dependent increase in radial stress is relatively small. Hypothetically, this could be due to a larger load causing greater damage at the contacts during loading, leaving the contacts less susceptible to further static fatigue.

The purpose of the tests presented in Fig. 11 was to collect evidence for contact maturing to be a plausible mechanism causing time effects in silica sand. The observed increase in radial stress in the soft oedometer under a sustained load is a manifestation of an increase in the macroscopic stiffness of sand caused possibly by maturing contacts. This was argued considering the elastic energy preservation in the ageing sand (equation (3)). In all cases in Fig. 11 the process appears to be decaying, but the rate depends on the type of sand and the pore fluid. The lowest rate of increase in the radial stress and settlement is displayed by a poorly graded, air-dry Ottawa sand (test A). Finer and better-graded Lake Michigan Empire Beach and dune sands (tests B and C, respectively) exhibit larger rates of radial stress increase. This is consistent with the hypothesis of contact maturing, where the finer sand has more contacts due to its finer grain content (even though the average contact force may be lower). A still larger increase in the rate of the ageing process is caused by the presence of pore fluid, and the resulting mineral dissolution at contacts. This is not surprising. The process of mineral dissolution at contacts (pressure dissolution) is likely to cause the evolution of contacts faster, leading to a higher rate of increase in the macroscopic stiffness, hence the faster increase in the radial stress. The process of silica dissolution is faster in highly alkaline solutions (Krauskopf, 1959), thus the faster increase in the radial stress in sodium hydroxide water solution with pH = 11 (test F) compared to the test with distilled water (test D). In geologic time, pressure dissolution is one of the processes leading to formation of sedimentary rock, also known as lithification.

The average inter-granular force in the specimens was about one order of magnitude smaller than the forces in the grain-scale convergence tests. However, the forces in the strong chains were likely to be of the same order. In both the

Table 2. Summary of soft oedometer tests

Test	Sand	Pore fluid	Porosity	Test duration: days	30 min after loading started		Radial stress increase		Time-dependent settlement	
					Radial stress: kPa	Settlement: μm	After 5 days: kPa	After 12 days: kPa	After 5 days: μm	After 12 days: μm
A	Ottawa	Air-dry	0·40	20	129·62	262·22	0·82	1·82	3·61	5·35
B	Beach*	Air-dry	0·38	12	118·90	563·17	2·92	3·57	8·19	9·95
C	Dune†	Air-dry	0·40	20	93·64	299·35	1·81	2·24	2·86	3·92
D	Ottawa	pH = 6·8‡	0·40	14	130·66	281·51	4·48	4·96	13·54	15·37
E§	Ottawa	pH = 6·8‡	0·40	20	174·60	355·53	2·46	3·47	17·25	21·04
F	Ottawa	pH = 11	0·40	20	144·88	467·12	8·15	10·75	19·57	26·07

*Lake Michigan Empire Beach sand.
†Lake Michigan dune sand.
‡distilled water.
§load: 345 kPa; all other tests: 230 kPa.

grain-scale and the oedometer tests, the process was most intense immediately after loading, with a significant drop in the gradient of convergence and the gradient of the radial stress increase after the first few days, to reach very small rates after 20 days. Only the grain with the largest initial roughness (RMS = 621 nm) and the Ottawa sand saturated with highly alkaline pore fluid (pH = 11) exhibited somewhat significant maturing/ageing after 20 days. These observations are consistent with the hypothesis indicating contact maturing as the key cause of ageing in silica sand.

Both the radial stress and settlement plots in Fig. 11 have some irregularities indicative of possible external excitation, or an electrical instability in the data collection system. These abrupt changes in reading data were found to be unavoidable. Most of them occurred within 1 s, therefore changes in temperature or humidity have been excluded from the possible causes. The accelerometer mounted on the oedometer frame indicated some disturbance during test D at about 7·5 and 8 days, but not in the remaining cases. Tests A and B were performed at the same time, and major 'steps' in radial stress and settlement readings were detected for both tests at the time of about 8 days. Abrupt changes in readings are also possible owing to the structuration events. These are instability events when grains assume new equilibrium positions, and are typically associated with some subsidence (Nadukuru *et al*., 2012).

FINAL REMARKS

Assemblies of sand grains are often modelled as systems of spheres (or grains of other shapes) with elastic contacts and a frictional limit on the inter-granular shear force. It was demonstrated in the paper that the contact behaviour is complex, owing to the elaborate morphology of the grain surfaces, and the time-dependent micro-fracturing process (static fatigue).

A qualitative grain-to-grain test in a spring-loaded micro-vice indicated time-dependent (but decaying) relative movement of two silica grains loaded with an oblique but constant force. Quantitative tests were carried out using a custom-designed apparatus. The authors advocated a hypothesis that the key cause of time effects in silica sand is the time-dependent fracturing of textural features (asperities) and mineral debris on grain surfaces at the contacts. This process was referred to as contact maturing, and it is especially distinct in fresh deposits and disturbed sand, where new contacts have been created. It was demonstrated that two loading platens forming contacts with a single grain, subjected to a constant force, undergo a process of convergence (the platens come closer together) that lasts weeks. This convergence is caused by maturing contacts. Under the loads considered (up to 2·4 N), grain fracture or crushing was not detected, but convergence due to creep of the grain core material was found to be noteworthy. Measurements of convergence were strongly dependent on the initial surface roughness of the grain. The convergence for a grain with a relatively high initial roughness (RMS = 621 nm), loaded with a force of 2·4 N, was 2·39 μm in the 20 days following the load application. This convergence drops with a decrease in roughness. For a grain with initial roughness of 321 nm, the 20 day convergence was 780 nm, and only 310 nm for a grain with initial RMS = 28·6 nm. The rate of the process is decaying, but is still strongly dependent on roughness in the first few days. The convergence rate was 17·6 nm/h at the end of the first day for a grain with initial RMS = 621 nm, but only a little above 2 nm/h for initial roughness of 321 nm, and below 2 nm/h for roughness of 28·6 nm. After 20 days, the convergence rate for all tests dropped below 1 nm/h, presumably with the substantial influence of creep of the grain core material.

The convergence test results are consistent with the contact maturing hypothesis. When the contact maturing process was negligible (in a test with a high-molybdenum stainless steel sphere), the time-dependent convergence was not detected.

The consequence of maturing of individual contacts in a confined assembly of grains is an increase in macroscopic stiffness. This results in a time-dependent increase in radial stress in oedometric specimens subjected to a sustained vertical load. Such an increase was detected in soft oedometer testing, and the intensity of this increase was found to be dependent on whether the specimen was air-dry or saturated with distilled water or an alkaline water solution. The latter causes substantial pressure dissolution at contacts, and therefore accelerated contact maturing and a faster increase in radial stress (and settlement). The temporal scales of the contact maturing process and the specimen-scale ageing process are similar, with both significantly reduced after about 20 days. When contact maturing was not present in the grain assembly (stainless steel spheres), no time-dependent increase in radial stress or settlement was present.

The test results presented are consistent with the hypothesis of contact maturing, which indicates time-dependent fracturing of microscopic textural features at contacts as the key cause of ageing in silica sand. The process is sensitive to environmental factors, and is accelerated in the presence of pore water, and even more so in the presence of high-pH solutions. As maturing of contacts has a decaying characteristic, the engineering consequences in 'aged' deposits may be insignificant; however,

the process is manifested distinctly in fresh deposits or in disturbed sand with newly formed contacts.

ACKNOWLEDGEMENTS

The work presented in this paper was supported by the National Science Foundation through grant CMMI-1537222. This support is greatly appreciated. The authors also would like to thank the College of Engineering of the University of Michigan, and the Michigan Center for Materials Characterization for use of the instruments and staff assistance.

NOTATION

E	Young's modulus
k	spring constant
m, n	number of rows and columns in a scanning field
W_e	elastic strain energy
z_{ij}	elevation of the point on grain surface located by row i and column j
μ	average elevation of the grain surface
ν	Poisson ratio
$\bar{\sigma}_r, \bar{\sigma}_z, \bar{\sigma}_\theta$	averaged stresses in a granular assembly in cylindrical coordinate system

REFERENCES

Afifi, S. S. & Woods, R. D. (1971). Long-term pressure effects on shear modulus of soils. *ASCE J. Soil Mech. Found. Div.* **97**, No. 10, 1445–1460.

Bažant, Z. P. & Pang, S. D. (2007). Activation energy based extreme value statistics and size effect in brittle and quasibrittle fracture. *J. Mech. Phys. Solids* **55**, No. 1, 91–131.

Bowman, E. T. & Soga, K. (2003). Creep, ageing and microstructural change in dense granular materials. *Soils Found.* **43**, No. 4, 107–117.

Brzesowsky, R. H., Hangx, S. J. T., Brantut, N. & Spiers, C. J. (2014). Compaction creep of sands due to time-dependent grain failure: effects of chemical environment, applied stress, and grain size. *J. Geophys. Res. Solid Earth* **119**, No. 10, 7521–7541.

Cavarretta, I., Coop, M. R. & O'Sullivan, C. (2010). The influence of particle characteristics on the behaviour of coarse grained soils. *Géotechnique* **60**, No. 6, 413–423, http://dx.doi.org/10.1680/geot.2010.60.6.413.

Cavarretta, I., Rocchi, I. & Coop, M. R. (2011). A new interparticle friction apparatus for granular materials. *Can. Geotech. J.* **48**, No. 12, 1829–1840.

Charles, S. J. (1958). Static fatigue of glass. I. *J. Appl. Physics* **29**, No. 11, 1549–1553.

Chow, F. C., Jardine, R. J., Brucy, F. & Nauroy, J. F. (1997). Time related increases in the shaft capacities of driven piles in sand. *Géotechnique* **47**, No. 2, 353–361, http://dx.doi.org/10.1680/geot.1997.47.2.353.

Cole, D. M. & Peters, J. F. (2008). Grain-scale mechanics of geologic materials and lunar simulants under normal loading. *Granular Matter* **10**, No. 3, 171–185.

Daramola, O. (1980). Effect of consolidation age on stiffness of sand. *Géotechnique* **30**, No. 2, 213–216, http://dx.doi.org/10.1680/geot.1980.30.2.213.

Einav, I. (2007). Breakage mechanics – part I: theory. *J. Mech. Physics Solids* **55**, No. 6, 1274–1297.

Glasstone, S., Laidler, K. J. & Eyring, H. (1941). *The theory of rate processes.* New York, NY, USA: McGraw-Hill.

Guo, R. & Hueckel, T. (2015). Silica polymer bonding of stressed silica grains: an early growth of intergranular tensile strength. *Geomech. Energy Environ.* **1**, 48–59.

Hu, L. B. & Hueckel, T. (2007). Coupled chemo-mechanics of intergranular contact: toward a three-scale model. *Comput. Geotech.* **34**, No. 4, 306–327.

Kolymbas, D. & Bauer, E. (1993). Soft oedometer – a new testing device and its application for the calibration of hypoplastic constitutive laws. *Geotech. Testing J.* **16**, No. 2, 263–270.

Krauskopf, K. B. (1959). The geochemistry of silica in sedimentary environments. In *Silica in sediments* (ed. H. A. Ireland), SP7, pp. 4–19. Tulsa, OK, USA: The Society of Economic Paleontologists and Mineralogists (SEPM).

Krausz, A. S. & Krausz, K. (1988). *Fracture kinetics of crack growth*. Boston, MA, USA: Kluwer.

Krumbein, W. C. (1941). Measurement and geological significance of shape and roundness of sedimentary particles. *J. Sediment. Res.* **11**, No. 2, 64–72.

Lade, P. V. & Karimpour, H. (2010). Static fatigue controls particle crushing and time effects in granular materials. *Soils Found.* **50**, No. 5, 573–583.

McDowell, G. R. & Bolton, M. D. (1998). On the micromechanics of crushable aggregates. *Géotechnique* **48**, No. 5, 667–679, http://dx.doi.org/10.1680/geot.1998.48.5.667.

Mesri, G., Feng, T. W. & Benak, J. M. (1990). Postdensification penetration resistance of clean sand. *J. Geotech. Engng* **116**, No. 7, 1095–1115.

Michalowski, R. L. & Nadukuru, S. S. (2012). Static fatigue, time effects, and delayed increase in penetration resistance after dynamic compaction of sand. *J. Geotech. Geoenviron. Engng* **138**, No. 5, 564–574.

Michalowski, R. L. & Nadukuru, S. S. (2014). Contact fatigue: a key mechanism of time effects in silica sand. In *Proceedings of IS-Cambridge 2014, geomechanics from micro to macro* (eds K. Soga, K. Kumar, G. Biscontin and M. Kuo), pp. 1201–1204. London, UK: Taylor & Francis.

Mitchell, J. K. & Solymar, Z. V. (1984). Time-dependent strength gain in freshly deposited or densified sand. *J. Geotech. Engng* **110**, No. 11, 1559–1576.

Nadukuru, S. S., O'Connor, S. M. & Michalowski, R. L. (2012). Static fatigue and delayed effects in sand and lunar regolith. In *Proceedings of ASCE earth and space 2012: engineering, science, construction, and operations in challenging environments* (eds K. Zacny, R. B. Malla and W. Binienda), pp. 256–263. Reston, VA, USA: American Society of Civil Engineers.

Rohe, A., Gareau, L. F. & Molenkamp, F. (2009). Lateral oedometer testing of anisotropic clay as affected by surface roughness. *Géotechnique* **59**, No. 8, 703–715, http://dx.doi.org/10.1680/geot.7.00158.

Savitzky, A. & Golay, M. J. E. (1964). Smoothing and differentiation of data by simplified least-squares procedures. *Analyt. Chem.* **36**, No. 8, 1627–1639.

Schmertmann, J. H. (1991). The mechanical aging of soils. *J. Geotech. Engng* **117**, No. 9, 1288–1330.

Scholz, C. H. (1972). Static fatigue of quartz. *J. Geophys. Res.* **77**, No. 11, 2104–2114.

Senetakis, K. & Coop, M. R. (2013). The development of a new micro-mechanical inter-particle loading apparatus. *Geotech. Testing J.* **37**, No. 6, 1–12.

Tatsuoka, F., Di Benedetto, H., Kongkitkul, W., Kongsukprasert, L., Nishi, T. & Sano, Y. (2008). Modelling of ageing effects on the elastic-viscoplastic behaviour of geomaterials. *Soils Found.* **48**, No. 2, 155–174.

Van Noort, R., Spiers, C. J. & Peach, C. J. (2011). Structure and properties of loaded silica contacts during pressure solution: impedance spectroscopy measurements under hydrothermal conditions. *Phys. Chem. Miner.* **38**, No. 7, 501–516.

Wang, Z. & Michalowski, R. L. (2015). Contact fatigue in silica sand – observations and modeling. *Geomech. Energy Environ.* **4**, 88–99.

Wang, Y. H., Gao, Y. & Ooi, G. L. (2016). Experimental characterizations of an aging mechanism of sands. *J. Geotech. Geoenviron. Engng* **142**, No. 2, 06015016.

Wiederhorn, S. M., Yi, F., LaVan, D., Richter, L. J., Fett, T. & Hoffmann, M. J. (2014). Volume expansion caused by water penetration into silica glass. *J. Am. Ceram. Soc.* **98**, No. 1, 78–87.

Zhao, B., Wang, J., Coop, M. R., Viggiani, G. & Jiang, M. (2015). An investigation of single sand particle fracture using X-ray micro-tomography. *Géotechnique* **65**, No. 8, 625–641, http://dx.doi.org/10.1680/geot.4.P.157.